

Bulk and surface modes in a one-dimensional gyro-uniaxial photonic crystalDaniele B. Provenzano * and Giuseppe C. la Rocca †
Faculty of Science, Scuola Normale Superiore, 56126 Pisa, Italy (Received 31 May 2024; accepted 28 August 2024; published 10 September 2024)

We examine the features of electromagnetic bulk and surface modes in a one-dimensional photonic crystal made up of lossless gyroelectric and uniaxial layers. We find a configuration that supports the propagation of a type of surface mode that can have either positive or negative group velocity, depending on the signs of the uniaxial permittivities. We also show how the introduction of gyrotropy qualitatively alters the photonic band structure, making it possible to modify the allowed frequency ranges within the structure just by varying the value of an external magnetic field. Exploiting an Otto configuration, we provide the analysis of a finite system where near-zero reflectivity values correspond to large Goos-Hänchen shifts. We also explore low-symmetry configurations where waves exhibit nonreciprocal behaviors.

DOI: [10.1103/PhysRevA.110.033514](https://doi.org/10.1103/PhysRevA.110.033514)**I. INTRODUCTION**

In the field of modern photonics, the intricate interplay between light and matter has opened the way for groundbreaking discoveries and technological advancements. In the past few decades, considerable attention has been focused on the properties of photonic crystals (PCs) [1,2], which is primarily due to their application in controlling the flow of light.

The optical properties of PCs are profoundly influenced by the characteristics of the media they are made of. In isotropic materials, neither wave polarization nor the refractive index depend on the direction of wave propagation. Conversely, in anisotropic materials such quantities may depend on the propagation direction. Such low-symmetry configurations lead to odd electromagnetic phenomena, such as Faraday rotation in gyrotropic media [3,4]. Consequently, PCs crafted from anisotropic materials exhibit markedly different characteristics compared to their isotropic counterparts. Notably, anisotropic PCs represent a rich resource due to their controllable dispersion, offering avenues for the creation of tunable optical devices [5–8]. By harnessing external electric or magnetic fields, such as those facilitated by liquid crystals, it becomes feasible to manipulate and adjust the properties of these PCs, including the opening, closing, or shifting of band gaps [9].

Beyond bulk modes, PCs harbor the potential to support the propagation of electromagnetic surface waves (ESWs). Such waves have garnered attention since Zenneck's work in [10]. These modes travel along interfaces separating two media while remaining localized in the transverse direction. Among the most notable examples of ESWs are surface plasmon polaritons (SPPs), characterized by a transverse magnetic (TM) nature, capable of propagating at the interface between two isotropic media with permittivities of opposite signs [11]. As

for interfaces involving gyrotropic media, ESWs show nonreciprocal features such as the asymmetry between forward and backward propagations [12–14]. In the context of periodic structures, prominent types of ESWs include Tamm waves and Bloch surface waves [15–24].

In this work we characterize bulk and surface waves that can propagate in a one-dimensional PC composed of lossless gyroelectric and uniaxial layers. While previous works have described light propagation in such two media separately [23,25], their combination has never been analyzed before. Our investigation reveals that, when the uniaxial components behave as hyperbolic materials (HMs), a new kind of ESW can propagate through the structure. Such modes exhibit either forward or backward propagation features, i.e., positive or negative group velocity, depending on the specific type of HM involved. This feature is pivotal for developing new photonic devices with controllable propagation directions for light. Moreover, we show that such waves have a much greater penetration depth into the bulk compared to Tamm waves and SPPs. It is well established that photonic crystals act as frequency filters, typically relying on bulk modes for this purpose. In our case, the significantly different penetration depths of SWs would allow control of signal transmission through surface modes rather than bulk modes.

We also show that the introduction of gyrotropy into the system significantly deforms the photonic bands. This suggests that the electromagnetic response of the realistic system could be tuned just by varying the value of the external magnetic field. In this way, one can freely modify the allowed frequency ranges within the structure.

We subsequently conduct a brief analysis of a finite system, composed of a few periods, where such effects can be found by looking at the reflection spectra using an Otto configuration. In this configuration, we show that near-zero values of the reflection coefficient correspond to nontrivial values of the Goos-Hänchen shift (GHS). Since the GHS is related to the excitation of SWs, it can be either positive or negative depending on the sign of the group velocity characterizing the

*Contact author: daniele.provenzano@sns.it

†Also at NEST, Piazza S. Silvestro 12, 56127 Pisa, Italy.

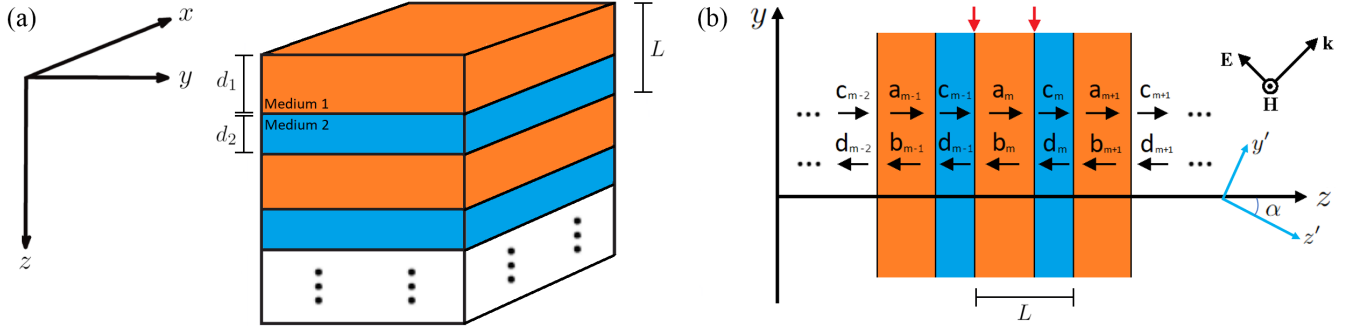


FIG. 1. (a) Outline of the one-dimensional periodic multilayer structure. (b) Outline of the yz plane section of the periodic structure under consideration. Here y' and z' represent the principal axes of the hyperbolic slabs

relative surface mode. Finally, we propose lower-symmetry configurations whose reflectivity is not symmetrical with respect to the inversion of the incidence angle, highlighting their nonreciprocal features due to gyrotropy.

II. ANISOTROPIC MULTILAYERED STRUCTURES

Let us consider a multilayered system consisting of an ordered succession of two lossless material slabs, whose thicknesses and dielectric tensors are d_1 , ϵ_1 and d_2 , ϵ_2 , respectively, as depicted in Fig. 1(a). Let the spatial periodicity of the stratified medium be $L = d_1 + d_2$ and \hat{z} be the growth direction such that the overall dielectric function on the structure can be written as

$$\epsilon = \begin{cases} \epsilon_1, & mL < z < mL + d_1 \\ \epsilon_2, & mL + d_1 < z < (m+1)L, \end{cases}$$

where m is an integer number. We consider a multilayered structure composed of gyroelectric and uniaxial layers such that their dielectric tensors read

$$\epsilon_1 = \epsilon_0 \begin{pmatrix} \epsilon_g & 0 & 0 \\ 0 & \epsilon_g & ig \\ 0 & -ig & \epsilon_g \end{pmatrix}, \quad \epsilon'_2 = \epsilon_0 \begin{pmatrix} \epsilon_{\perp} & 0 & 0 \\ 0 & \epsilon_{\parallel} & 0 \\ 0 & 0 & \epsilon_{\perp} \end{pmatrix} \quad (1)$$

in their respective principal coordinate systems. As for the uniaxial medium, let us initially consider the general

$$H_x^m(y, z) = \begin{cases} [a_m e^{ik_u(z-mL)} + b_m e^{-ik_u(z-mL)}] e^{i(k_y y - \omega t)} & mL < z < mL + d_u, \\ [c_m e^{ik_g(z-mL)} + d_m e^{-ik_g(z-mL)}] e^{i(k_y y - \omega t)} & mL + d_u < z < (m+1)L, \end{cases} \quad (2)$$

where u stands for uniaxial and g for gyrotropic, k_u and k_g represent the z components of the wave vectors, and $L \equiv d_u + d_g$ is the period of the structure, with d_u and d_g the thicknesses of the two slabs, respectively. The coefficients a_m , b_m , c_m , and d_m are the amplitudes of forward and backward modes relative to each medium, as outlined in Fig. 1(b).

Applying the continuity conditions for H_x and E_y on the two boundaries marked by red arrows in Fig. 1(b) leads to a four-equation system relating the six variables a_m , b_m , c_m , d_m , c_{m-1} , and d_{m-1} . As shown in the Appendix, the whole algebraic system can be recast in order to express c_{m-1} and

configuration wherein its optical axis is neither parallel nor perpendicular to the interface between the two media. Hence, we have to rotate its dielectric tensor by means of a rotation matrix such that, in our coordinate system, the uniaxial dielectric tensor reads

$$\epsilon_2 = \mathbf{R}_x(\alpha) \epsilon'_u \mathbf{R}_x(-\alpha) = \epsilon_0 \begin{pmatrix} \epsilon_{xx} & 0 & 0 \\ 0 & \epsilon_{yy} & \epsilon_{yz} \\ 0 & \epsilon_{zy} & \epsilon_{zz} \end{pmatrix},$$

where the matrix elements are

$$\begin{aligned} \epsilon_{xx} &= \epsilon_{\perp}, \\ \epsilon_{yy} &= \epsilon_{\perp} \sin^2 \alpha + \epsilon_{\parallel} \cos^2 \alpha, \\ \epsilon_{yz} &= \epsilon_{zy} = (\epsilon_{\perp} - \epsilon_{\parallel}) \sin \alpha \cos \alpha, \\ \epsilon_{zz} &= \epsilon_{\perp} \cos^2 \alpha + \epsilon_{\parallel} \sin^2 \alpha. \end{aligned}$$

For analytical convenience, we focus on anisotropic configurations where TE and TM modes can be decoupled, while low-symmetry configurations will be numerically investigated in Sec. V. Nontrivial results will concern only the TM polarization; thus it is appropriate to consider the following form for the magnetic field, accounting for both forward and backward modes:

d_{m-1} as functions of c_m and d_m ,

$$\begin{pmatrix} c_{m-1} \\ d_{m-1} \end{pmatrix} = \begin{pmatrix} A & B \\ C & D \end{pmatrix} \begin{pmatrix} c_m \\ d_m \end{pmatrix}, \quad (3)$$

where A , B , C , and D are complex coefficients, which will be derived in the next section. We will use this formalism in order to find the eigenmodes in a one-dimensional periodic structure.

III. ANISOTROPIC PHOTONIC CRYSTALS

If we let the number of layers become infinite, we obtain a photonic crystal. In such a periodic system, the Bloch theorem assures that the solution to the Helmholtz equation is a Bloch wave, namely, a wave function which can be written as the product of a plane wave and a periodic term

$$\mathbf{H}(z) = \mathbf{H}_B(z)e^{iK_B z}, \quad (4)$$

where $\mathbf{H}_B(z) = \mathbf{H}_B(z + L)$ is a periodic function and K_B is the Bloch wave number [26]. Following the procedure shown in [27], we must solve the eigenvalue problem

$$\begin{pmatrix} A & B \\ C & D \end{pmatrix} \begin{pmatrix} c_m \\ d_m \end{pmatrix} = e^{-iK_B L} \begin{pmatrix} c_m \\ d_m \end{pmatrix}, \quad (5)$$

whose solutions are

$$\begin{pmatrix} c_m \\ d_m \end{pmatrix} = \begin{pmatrix} B \\ e^{-iK_B L} - A \end{pmatrix}, \quad (6)$$

where

$$K_B = \pm \frac{1}{L} \cos^{-1} \left(\frac{A + D}{2} \right). \quad (7)$$

As pointed out in the Appendix, the eigenvalues are the reciprocals of each other because the matrix in Eq. (5) is unitary. If K_B is a real number, the eigenvalues represent propagating waves, whereas complex values of K_B correspond to damped waves in the bulk. Due to the properties of the cosine function, we can distinguish two scenarios: If $A + D \in \mathbb{R}$ and $A + D < 2$, the Bloch wave can propagate through the PC; otherwise it will decay inside the bulk [26,27]. The latter situation corresponds to the band gap.

We can derive the coefficients A , B , C , and D in the TM case by means of Eqs. (A1)–(A4). By defining

$$\epsilon_v \equiv \frac{\epsilon_g^2 - g^2}{\epsilon_g}$$

and

$$Z \equiv \frac{\epsilon_{yz}\epsilon_v}{\epsilon_{\parallel}\epsilon_{\perp}} - i \frac{g}{\epsilon_g}, \quad (8)$$

they turn out to be

$$A_{\text{TM}} = e^{ik_u d_u} \left[\cos k_g d_g + \frac{i}{2} \sin k_g d_g \left(\frac{\epsilon_{\parallel}\epsilon_{\perp}k_g}{\epsilon_v\epsilon_{zz}k_u} + \frac{\epsilon_v\epsilon_{zz}k_u}{\epsilon_{\parallel}\epsilon_{\perp}k_g} - \frac{\epsilon_{\parallel}\epsilon_{\perp}}{\epsilon_v\epsilon_{zz}} \frac{k_y^2}{k_u k_g} Z^2 \right) \right], \quad (9)$$

$$B_{\text{TM}} = \frac{i}{2} e^{-ik_u d_u} \sin k_g d_g \left(\frac{\epsilon_{\parallel}\epsilon_{\perp}k_g}{\epsilon_v\epsilon_{zz}k_u} - \frac{\epsilon_v\epsilon_{zz}k_u}{\epsilon_{\parallel}\epsilon_{\perp}k_g} - \frac{\epsilon_{\parallel}\epsilon_{\perp}}{\epsilon_v\epsilon_{zz}} \frac{k_y^2}{k_u k_g} Z^2 + 2Z \frac{k_y}{k_g} \right), \quad (10)$$

$$C_{\text{TM}} = -\frac{i}{2} e^{ik_u d_u} \sin k_g d_g \left(\frac{\epsilon_{\parallel}\epsilon_{\perp}k_g}{\epsilon_v\epsilon_{zz}k_u} - \frac{\epsilon_v\epsilon_{zz}k_u}{\epsilon_{\parallel}\epsilon_{\perp}k_g} - \frac{\epsilon_{\parallel}\epsilon_{\perp}}{\epsilon_v\epsilon_{zz}} \frac{k_y^2}{k_u k_g} Z^2 - 2Z \frac{k_y}{k_g} \right), \quad (11)$$

$$D_{\text{TM}} = e^{-ik_u d_u} \left[\cos k_g d_g - \frac{i}{2} \sin k_g d_g \left(\frac{\epsilon_{\parallel}\epsilon_{\perp}k_g}{\epsilon_v\epsilon_{zz}k_u} + \frac{\epsilon_v\epsilon_{zz}k_u}{\epsilon_{\parallel}\epsilon_{\perp}k_g} - \frac{\epsilon_{\parallel}\epsilon_{\perp}}{\epsilon_v\epsilon_{zz}} \frac{k_y^2}{k_u k_g} Z^2 \right) \right]. \quad (12)$$

Note that Z reduces to zero if both media are isotropic and, consequently, the matrix elements (9)–(12) reduce to the expressions commonly documented in the literature [1,26,27]. Furthermore, Eq. (7) becomes

$$K_{\text{TM}}^B = \frac{1}{L} \cos^{-1} (\cos k_g d_g \cos k_u d_u - \mathcal{F} \sin k_g d_g \sin k_u d_u), \quad (13)$$

where we defined

$$2\mathcal{F} \equiv \frac{\epsilon_{\parallel}\epsilon_{\perp}k_g}{\epsilon_v\epsilon_{zz}k_u} + \frac{\epsilon_v\epsilon_{zz}k_u}{\epsilon_{\parallel}\epsilon_{\perp}k_g} - \frac{\epsilon_{\parallel}\epsilon_{\perp}}{\epsilon_v\epsilon_{zz}} \frac{k_y^2}{k_u k_g} Z^2. \quad (14)$$

As mentioned in the preceding section, we only focus on TM polarization because TE modes obey the very same equations as in the isotropic case.

Before moving on, it is essential to make a significant observation. As evident from Eqs. (13) and (14), the presence of Z ensures that K_B has an imaginary part if $g \neq 0$ and $\epsilon_{yz} \neq 0$ simultaneously, for any real values of ω and k_y . This is surprising, especially considering that it holds true even for lossless structures, such as the ones we aim to analyze. In any case, the band diagram is almost empty because, apart

from normal incidence and a few other cases, no mode can propagate into the bulk. This last statement will be further examined during the discussion of the numerical results. We aim to investigate nontrivial scenarios involving gyrotropy; hence we are compelled to restrict our analysis to the case $\alpha = k\pi/2$, where $k \in \mathbb{Z}$.

In the next section we employ Eq. (13) to derive band diagrams for TM modes within our anisotropic PC. Our objective is to identify surface states within the band gaps, where bulk modes are not allowed to propagate.

IV. MODES IN A SEMI-INFINITE PHOTONIC CRYSTAL

Valuable insights can be gathered by exploring the surface modes permitted to propagate in PCs [17,28], as we demonstrate below.

When a PC is cut along one interface between two consecutive slabs, two semi-infinite PCs are created. The dispersion relation for surface waves propagating on a semi-infinite PC bordering a dielectric half space is [18,22]

$$e^{iK_B L} - A - \frac{Bc}{\omega\epsilon_I} \sqrt{\epsilon_I \left(\frac{\omega}{c} \right)^2 - k_y^2} = 0, \quad (15)$$

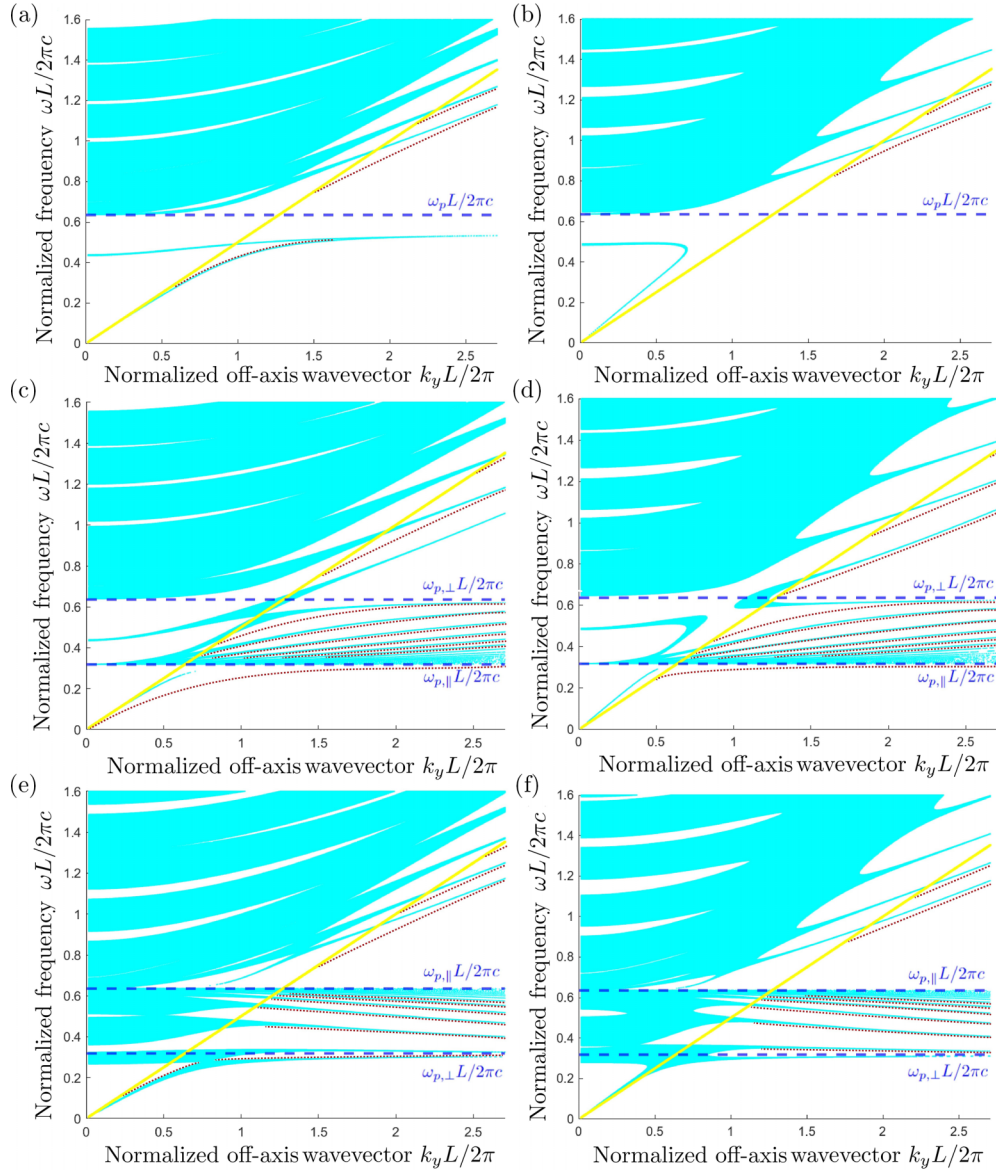


FIG. 2. Reduced band diagrams for TM waves in a metal-dielectric PC, for different values of the structural parameters. The red dotted lines correspond to surface modes, whereas the yellow solid line represents the light line of the dielectric half space. The structural parameters considered are $\epsilon_l = 4$, $\epsilon_g = 3$, $\epsilon_\infty = 8$, $d_g = 0.56 \mu\text{m}$, $d_u = 0.44 \mu\text{m}$, and $\alpha = \pi/2$. The other parameters are (a) $\omega_{p,\parallel} = \omega_{p,\perp}$ and $g = 0$, (b) $\omega_{p,\parallel} = \omega_{p,\perp}$ and $g = 1.5$, (c) $\omega_{p,\parallel} < \omega_{p,\perp}$ and $g = 0$, (d) $\omega_{p,\parallel} < \omega_{p,\perp}$ and $g = 1.5$, (e) $\omega_{p,\parallel} > \omega_{p,\perp}$ and $g = 0$, and (f) $\omega_{p,\parallel} > \omega_{p,\perp}$ $g = 1.5$.

where ϵ_l is the dielectric constant of the isotropic dielectric half space. Equation (15) enables us to identify and graphically represent the surface modes directly on the reduced band diagrams that characterize the system.

Prior to presenting our numerical findings, it is important to introduce the frequency dependence of the dielectric functions. We choose to consider the following dispersion for the uniaxial medium permittivities:

$$\epsilon_{\perp,\parallel} = \epsilon_\infty \left(1 - \frac{\omega_{p,\perp,\parallel}^2}{\omega^2} \right). \quad (16)$$

Such response functions with anisotropic plasma frequencies characterize the behavior of media that exist in nature [29,30] or can be artificially engineered using multilayer or nanowire

array geometries [31–33]. In such engineered media, nonlocal effects may play a significant role in shaping the dispersion of electromagnetic waves, as discussed in [34,35]. We neglect such effects in the present work.

As ω varies, Eq. (16) may describe an anisotropic metal [$\omega < \min(\omega_{p,\perp}, \omega_{p,\parallel})$], an anisotropic dielectric [$\omega > \max(\omega_{p,\perp}, \omega_{p,\parallel})$], or a hyperbolic medium [$\min(\omega_{p,\perp}, \omega_{p,\parallel}) < \omega < \max(\omega_{p,\perp}, \omega_{p,\parallel})$]. The last regime is of particular interest when it comes to surface modes, as shown in Fig. 2 for three different scenarios $\omega_{p,\parallel} = \omega_{p,\perp}$ [Figs. 2(a) and 2(b)], $\omega_{p,\parallel} < \omega_{p,\perp}$ [Figs. 2(c) and 2(d)], and $\omega_{p,\parallel} > \omega_{p,\perp}$ [Figs. 2(e) and 2(f)] for nongyrotropy [Figs. 2(a), 2(c), and 2(e)] and gyroelectric [Figs. 2(b), 2(d), and 2(f)] cases. It should be specified that the surface modes in Fig. 2 only concern the configuration where the semi-infinite crystal terminates with

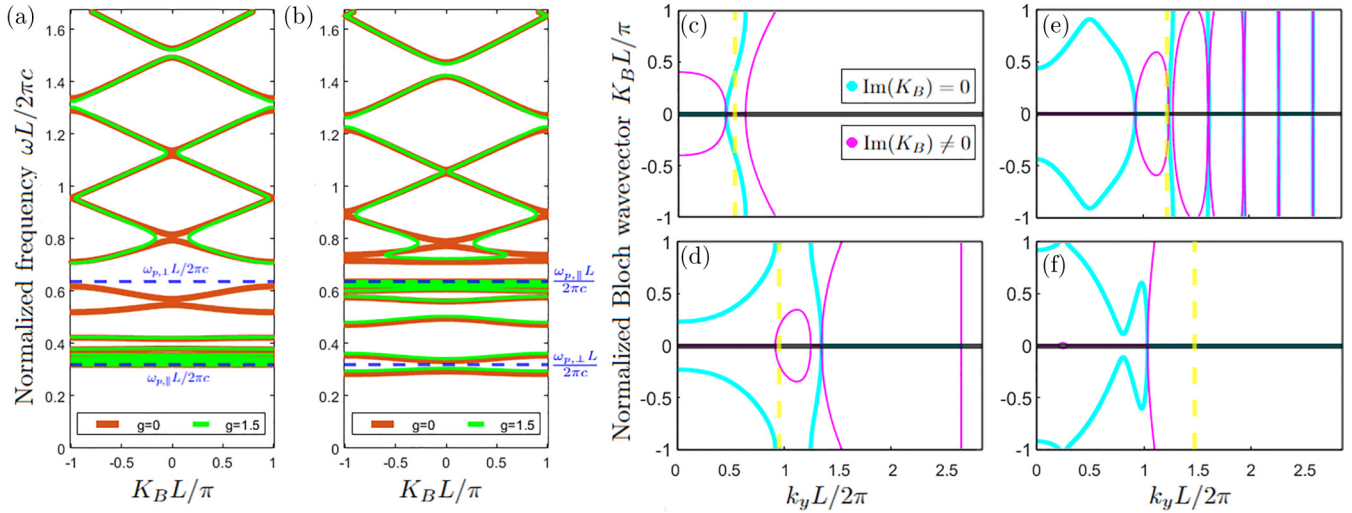


FIG. 3. Transversal sections of the reduced band diagram shown in Fig. 2, for $k_y L/2\pi = 1$, corresponding to (a) Figs. 2(c) and 2(d) and (b) Figs. 2(e) and 2(f). As gyrotropy is switched on, a large number of bulk bands appear slightly above or below the $\omega_{p,\parallel} L/2\pi c$ line. Also shown are the isofrequency contours corresponding to four slices of Fig. 2(f) at (c) $\omega L/2\pi c = 0.27$, (d) $\omega L/2\pi c = 0.48$, (e) $\omega L/2\pi c = 0.61$, and (f) $\omega L/2\pi c = 0.74$. Thick cyan curves represent bulk bands, whereas thin magenta lines correspond to complex values of the Bloch wave vector. Yellow dashed lines represents light lines.

a gyrotropic slab. If this were not the case, the dispersion of the surface waves would be slightly different, but all their characteristic features would remain the same.

For the case in Figs. 2(a) and 2(b), $\omega_{p,\parallel} = \omega_{p,\perp} \equiv \omega_p$, two distinct types of surface waves are observed: a truncated SPP below the threshold $\omega = \omega_p$ and Tamm waves in the domain $\omega > \omega_p$, where the metallic constituents demonstrate dielectric behavior ($\epsilon_{\parallel}, \epsilon_{\perp} > 0$). When gyrotropy is switched on within the dielectric layers, the lower bands get modified such that the SPP no longer exists. Conversely, Tamm waves experience subtle modifications but do not undergo significant alterations.

For the case in Figs. 2(c) and 2(d), $\omega_{p,\parallel} < \omega_{p,\perp}$, the horizontal bulk plasmon line undergoes a significant division into numerous bulk bands, situated within the range delineated by the plasma frequencies $\omega_{p,\parallel}$ and $\omega_{p,\perp}$, where the anisotropic metallic components behave as type 2 hyperbolic metamaterials (HMMs) [36,37]. Notably, an intermediate surface mode emerges within each band gap separating the bulk bands. These waves have a positive group velocity; thus they propagate in the forward direction. Interestingly, the introduction of gyrotropy has minimal impact on surface modes, despite some degenerate bands undergoing division. For enhanced clarity, Fig. 3(a) illustrates two transversal sections of the reduced band diagram.

For the case in Figs. 2(e) and 2(f), $\omega_{p,\parallel} > \omega_{p,\perp}$, similar to the previous scenario, an infinite array of bulk bands occupies the domain delineated by the plasma frequencies $\omega_{p,\perp}$ and $\omega_{p,\parallel}$. Within this domain, the anisotropic metallic components behave as type 1 HMMs [36,37]. Notably, all the intermediate surface waves demonstrate a negative group velocity, implying their propagation in the backward direction. Furthermore, the SPP undergoes bifurcation into two branches due to the convergence of lower bands. When gyrotropy is switched on, the lower bands get modified such that the SPP no longer exists. For enhanced clarity, Fig. 3(b) illustrates two transversal

sections of the reduced band diagrams, whereas Figs. 3(c)–3(f) show four isofrequency contours in the gyrotropic case.

In summary, these intermediate waves¹ can propagate either forward or backward, depending on the hyperbolic behavior of the uniaxial material constituting the structure. Similar results were found in [38] for the nongyrotropic case. In such work, the intermediate surface modes are referred to as Tamm-Langmuir surface waves.

As previously stated, the presence of gyrotropy in the system modifies some bulk bands, as can be clearly seen in Fig. 3. This implies that by adjusting the external magnetic field, the electromagnetic response of the system can be fine-tuned, allowing for the modification of the permissible frequency ranges within the structure.

Figure 4 presents a comparison of the field distributions between the Tamm wave and the intermediate mode. Notably, the latter exhibits a significantly greater penetration depth than the former. This property may allow the control of signal transmission through surface modes rather than bulk modes. It is observed that the electric field of the novel modes concentrates and oscillates within the uniaxial metallic layers. This unique feature facilitates deeper penetration of the mode into the bulk. Such a behavior is common to layered periodic metal-dielectric structures with anisotropic metal layers [39] and does not depend on the presence of a gyrotropic medium.

We conclude this section by numerically investigating the observation made at the end of Sec. III, concerning the restriction to $\alpha = k\pi/2$, where $k \in \mathbb{Z}$. As pointed out before, if $\alpha \neq k\pi/2$ then the Bloch wave number is complex almost for every nonzero value of k_y . As further confirmation, Fig. 5 shows the behavior of the imaginary part of K_B as k_y varies,

¹The word *intermediate* refers to the position of the new surface modes, which exist in the frequency domain delimited by the two plasma frequencies.

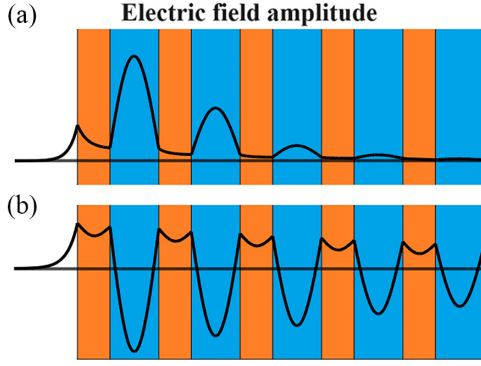


FIG. 4. Typical space distributions of the y component of the electric-field amplitude in a semi-infinite gyro-uniaxial PC. The blue regions represent the uniaxial components, whereas the orange regions represent the gyrotropic components. (a) Tamm wave. (b) Intermediate surface mode.

for four different values of the working frequency. It is evident that $K_B \in \mathbb{C}$ almost everywhere. Note that, depending on the working frequency, the imaginary part of K_B may be huge or approach zero at normal incidence. The first case corresponds to the band gap, where $A + D$ is now real but larger than 2. The second case corresponds to bulk propagating modes; hence this demonstrates that the band diagram is not empty at normal incidence. Moreover, apart from the case $k_y \rightarrow 0$, there may exist further values of k_y for which $\text{Im}(K_B)$ becomes very small. This is due to the form of Eq. (14): k_u and k_g are imaginary for high values of the off-axis wave vector; hence the imaginary part of the coefficient \mathcal{F} can actually become zero for a limited number of values of k_y .

V. FINITE MULTILAYER STRUCTURES

This section contains a few numerical results concerning finite structures, whose properties were analyzed using the so-called Otto configuration with a coupling prism whose refractive index is 3. As for the numerical method, we used the 4×4 transfer matrix formalism for anisotropic media, proposed by Berreman [40].

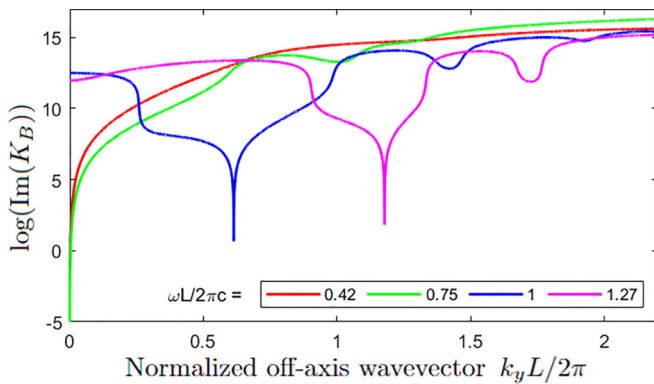


FIG. 5. Natural logarithm of the imaginary part of the Bloch wave number as a function of the off-axis wave vector, for four different values of the working frequency. The structural parameters are the same as in Fig. 2(d), except for $\alpha = 1$ rad.

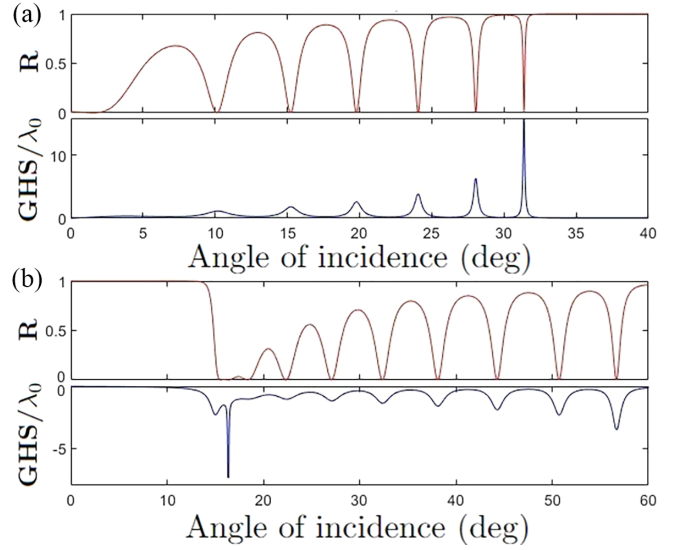


FIG. 6. Reflectivity and Goos-Hänchen shift (in units of the incident wavelength) for two multilayer structures composed of ten periods, calculated using the transfer matrix method. The structural parameters are the same as in Fig. 2. The other parameters are (a) $\omega_{p,\parallel} < \omega_{p,\perp}$, corresponding to forward surface modes of Fig. 2(d), and (b) $\omega_{p,\parallel} > \omega_{p,\perp}$, corresponding to backward-propagating surface modes of Fig. 2(f).

First, we conducted a brief analysis on the Goos-Hänchen shift [41] for finite multilayer structures. It is well known that the GHS dramatically increases when getting close to the Brewster angle [42], at which light is totally transmitted through the system. We calculated both the reflectivity and the GHS for two structures consisting of ten periods each, in the frequency domain delimited by the two plasma frequencies $\omega_{p,\perp}$ and $\omega_{p,\parallel}$. The results are shown in Fig. 6. Consistent with expectations, at angles where the reflectivity approaches zero, the GHS is positive in the case of forward modes, whereas it is negative for backward modes.

A final matter worth consideration is bulk bands. As can be seen from Eqs. (13) and (14), the dispersion of bulk bands only depends on k_y^2 ; hence there is no difference between positive and negative angles of incidence. Indeed, the bulk modes are not affected by nonreciprocity effects despite the presence of a gyrotropic medium. One way to break the high level of symmetry and be able to observe differences between positive and negative angles of incidence is to rotate the gyroelectric components such that, in our coordinate system, their dielectric tensor reads

$$\epsilon_1 = \epsilon_0 \begin{pmatrix} \epsilon_g & 0 & ig \\ 0 & \epsilon_g & 0 \\ -ig & 0 & \epsilon_g \end{pmatrix}. \quad (17)$$

Figure 7 shows a comparison between the reflectivity of two multilayer structures whose gyrotropic tensors are described by Eqs. (1) and (17). It appears evident that the latter configuration introduces asymmetry between positive and negative angles of incidence. Such a configuration cannot be analyzed using the method of Sec. III because TE and TM modes cannot be decoupled. They should be studied at the same time.

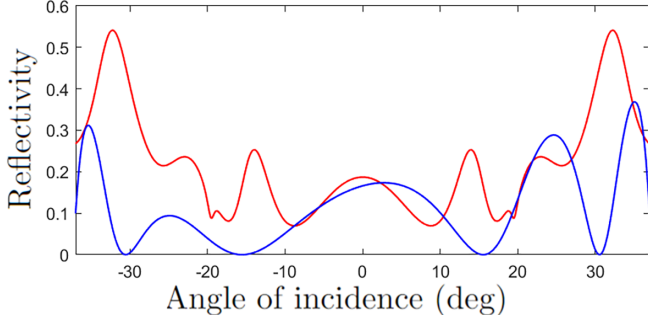


FIG. 7. Comparison between the reflectivity of gyro-uniaxial multilayer structures whose gyrotropic components are described by Eq. (1) (red symmetric curve) and Eq. (17) (blue asymmetric curve).

VI. CONCLUSION

We have employed an analytical method to characterize the dispersion of bulk bands and surface states in a one-dimensional PC composed of lossless gyroelectric and uniaxial layers. This study reveals that the structure can support not only SPPs and Tamm waves, but also a new kind of ESW. These surface waves exhibit either positive or negative group velocity, which is crucial for developing new photonic devices with controllable light propagation directions. Our analysis shows that these surface waves have a much greater penetration depth into the bulk compared to Tamm waves and SPPs. This significant difference in penetration depths allows for controlling signal transmission through surface modes rather than bulk modes, enhancing the functionality of photonic crystals as frequency filters. Furthermore, the introduction of gyrotropy into the system significantly deforms the photonic bands, indicating that the electromagnetic response can be finely tuned by varying the external magnetic field. This ability to modify the allowed frequency ranges within the structure enhances the versatility of PCs. We also explored the reflectivity spectra of finite structures arranged in an Otto configuration. Near-zero reflectivity values correspond to high values of the Goos-Hänchen shift, which can be either positive or negative depending on the sign of the group velocity characterizing the relative surface mode. Additionally, we examined configurations with asymmetrical reflectivity with respect to the inversion of the incidence angle, highlighting their nonreciprocal features due to gyrotropy.

Overall, our findings underscore the potential for controlling signal transmission through novel surface modes in layered structures based on a combination of hyperbolic and gyroelectric media capitalizing on the properties of both material classes.

APPENDIX: INTERFACE CONDITIONS

Given H_x in Eq. (2), it is trivial to evaluate E_y and E_z by means of Maxwell's equations. Additionally, they imply that H_x and E_y are continuous functions along the boundaries, while E_z is not, due to the dielectric function's discontinuity. The continuity of both H_x and E_y on the two boundaries marked by red arrows in Fig. 1(b) leads to

$$c_{m-1} + d_{m-1} = a_m e^{ik_g L} + b_m e^{-ik_g L}, \quad (\text{A1})$$

$$c_m e^{ik_u d_u} + d_m e^{-ik_u d_u} = a_m e^{ik_g d_u} + b_m e^{-ik_g d_u}, \quad (\text{A2})$$

$$\frac{i\epsilon_v}{\epsilon_{\parallel}\epsilon_{\perp}} [d_{m-1}(\epsilon_{zz}k_u + \epsilon_{zz}k_y) + c_{m-1}(\epsilon_{zz}k_y - \epsilon_{zz}k_u)] = a_m \left(ik_g - \frac{g}{\epsilon_g} k_y \right) e^{ik_g L} - b_m \left(ik_g + \frac{g}{\epsilon_g} k_y \right) e^{-ik_g L}, \quad (\text{A3})$$

$$\frac{i\epsilon_v e^{ik_u d_u}}{\epsilon_{\parallel}\epsilon_{\perp}} [c_m(\epsilon_{zz}k_u + \epsilon_{yz}k_y) + d_m(\epsilon_{yz}k_y - \epsilon_{zz}k_u) e^{-2ik_u d_u}] = a_m \left(ik_g - \frac{g}{\epsilon_g} k_y \right) e^{ik_g d_u} - b_m \left(ik_g + \frac{g}{\epsilon_g} k_y \right) e^{-ik_g d_u}, \quad (\text{A4})$$

where we defined

$$\epsilon_v \equiv \frac{\epsilon_g^2 - g^2}{\epsilon_g}.$$

The components of the wave vectors obey the following dispersion relations:

$$\epsilon_{yy}k_y^2 + \epsilon_{zz}k_u^2 + 2k_y k_u \epsilon_{yz} = \frac{\omega^2}{c^2} \epsilon_{\parallel}\epsilon_{\perp},$$

$$k_g^2 + k_y^2 = \epsilon_v \frac{\omega^2}{c^2}.$$

Let us use a_m and b_m as free variables and recast the system (A1)–(A4) into the form

$$\begin{pmatrix} c_{m-1} \\ d_{m-1} \end{pmatrix} = \mathbf{P}^{-1} \mathbf{Q} \begin{pmatrix} a_m \\ b_m \end{pmatrix}, \quad \begin{pmatrix} c_m \\ d_m \end{pmatrix} = \mathbf{R}^{-1} \mathbf{S} \begin{pmatrix} a_m \\ b_m \end{pmatrix},$$

where \mathbf{P} , \mathbf{Q} , \mathbf{R} , and \mathbf{S} are 2×2 matrices [27]. The two preceding equations imply

$$\begin{pmatrix} c_{m-1} \\ d_{m-1} \end{pmatrix} = \mathbf{P}^{-1} \mathbf{Q} \mathbf{S}^{-1} \mathbf{R} \begin{pmatrix} c_m \\ d_m \end{pmatrix}. \quad (\text{A5})$$

The matrix

$$\mathbf{P}^{-1} \mathbf{Q} \mathbf{S}^{-1} \mathbf{R} \equiv \begin{pmatrix} A & B \\ C & D \end{pmatrix}$$

is unimodular because it relates the field amplitudes of equivalent layers of two consecutive cells [26,27].

- [1] J. D. Joannopoulos, S. G. Johnson, J. N. Winn, and R. D. Meade, *Photonic Crystals: Molding the Flow of Light*, 2nd ed. (Princeton University Press, Princeton, 2011).
 [2] *Photonic Crystals: Physics, Fabrication and Applications*, edited by K. Inoue and K. Ohtaka, Springer Series in Optical Sciences (Springer, Berlin, 2004), Vol. 94.

- [3] L. D. Landau and E. M. Lifshitz, *Electrodynamics of Continuous Media* (Pergamon, Oxford, 1984).
 [4] A. Zangwill, *Modern Electrodynamics* (Cambridge University Press, Cambridge, 2012).
 [5] G. Alagappan, X. W. Sun, P. Shum, M. B. Yu, and D. den Engelsen, Symmetry properties of two-dimensional

- anisotropic photonic crystals, *J. Opt. Soc. Am. A* **23**, 2002 (2006).
- [6] G. Alagappan, X. W. Sun, P. Shum, M. B. Yu, and M. T. Doan, One-dimensional anisotropic photonic crystal with a tunable bandgap, *J. Opt. Soc. Am. B* **23**, 159 (2006).
- [7] V. I. Fesenko, I. A. Sukhoivanov, S. N. Shulga, and H. Shi, in *Proceedings of the 2008 12th International Conference on Mathematical Methods in Electromagnetic Theory* (IEEE, Piscataway, 2008), pp. 457–459.
- [8] K. Vytovtov and L. Mospan, in *Proceedings of the 2011 41st European Microwave Conference, Manchester* (EuMA, Louvain-la-Neuve, 2011), pp. 818–821.
- [9] S. Kim and S. Kurihara, in *Theoretical Foundations and Application of Photonic Crystals*, edited by A. Vakhruhev (InTech, London, 2018).
- [10] J. Zenneck, Über die fortpflanzung ebener elektromagnetischer Wellen längs einer ebenen leiterfläche und ihre Beziehung zur drahtlosen Telegraphie, *Ann. Phys. (Leipzig)* **328**, 846 (1907).
- [11] S. A. Maier, *Plasmonics: Fundamentals and Applications* (Springer, New York, 2007).
- [12] R.-L. Chern and Y.-Z. Yu, Chiral surface waves on hyperbolic-gyromagnetic metamaterials, *Opt. Express* **25**, 11801 (2017).
- [13] D. B. Provenzano and G. C. la Rocca, Interface mode between gyroelectric and hyperbolic media, *J. Opt. Soc. Am. B* **40**, 172 (2023).
- [14] Y. Zheng, J. Chen, Z. Ji, H. Lin, and Z.-Y. Li, Analytical solutions for electromagnetic surface states at the interface between metal and gyromagnetic media, *J. Opt. Soc. Am. B* **40**, 2815 (2023).
- [15] A. Lakhtakia, T. Mackay, and C. Zhou, Electromagnetic surface waves at exceptional points, *Eur. J. Phys.* **42**, 015302 (2020).
- [16] J. A. Polo Jr., T. G. Mackay, and A. Lakhtakia, *Electromagnetic Surface Waves: A Modern Perspective* (Elsevier, Amsterdam, 2013).
- [17] J. Bashiri, B. Rezaei, J. Barvestani, and C. J. Zapata-Rodríguez, Bloch surface waves engineering in one-dimensional photonic crystals with a chiral cap layer, *J. Opt. Soc. Am. B* **36**, 2106 (2019).
- [18] T.-B. Wang, C. Yin, W.-Y. Liang, J.-W. Dong, and H.-Z. Wang, Electromagnetic surface modes in one-dimensional photonic crystals with dispersive metamaterials, *J. Opt. Soc. Am. B* **26**, 1635 (2009).
- [19] A. Akjouj, E. B. El Houssaine, L. Dobrzynski, B. Djafari-Rouhani, and G. Lévêque, *Photonics* (Elsevier, Amsterdam, 2021), Pt. 3, pp. 489–527.
- [20] J. Martorell, D. W. L. Sprung, and G. V. Morozov, Surface TE waves on 1D photonic crystals, *J. Opt. A* **8**, 630 (2006).
- [21] J. Barvestani, M. Kalafi, and A. Vala, Surface optical waves in semi-infinite one-dimensional photonic crystals containing alternating layers of positive and negative media with a cap layer, *Acta Phys. Pol. A* **112**, 1089 (2007).
- [22] S. Feng, H.-Y. Sang, Z.-Y. Li, B.-Y. Cheng, and D.-Z. Zhang, Sensitivity of surface states to the stack sequence of one-dimensional photonic crystals, *J. Opt. A* **7**, 374 (2005).
- [23] E. E. Narimanov, Photonic hypercrystals, *Phys. Rev. X* **4**, 041014 (2014).
- [24] J. S. Pérez-Huerta, P. Lopez, W. Mochán, G. Ortiz, V. Agarwal, and R. Castro-García, Reflectivity of 1D photonic crystals: A comparison of computational schemes with experimental results, *Int. J. Mod. Phys. B* **32**, 1850136 (2018).
- [25] X. Zhao, Y. Luo, and L. Zhou, in *Proceedings of the 2007 International Nano-Optoelectronics Workshop* (IEEE, Piscataway, 2007), pp. 144–145.
- [26] A. Yariv and P. Yeh, *Optical Waves in Crystals: Propagation and Control of Laser Radiation* (Wiley, New York, 2002).
- [27] P. Yeh, *Optical Waves in Layered Media* (Wiley, New York, 2005).
- [28] A. Vinogradov, A. Dorofeenko, A. Merzlikin, and A. Lisyansky, Surface states in photonic crystals, *Phys. Usp.* **53**, 243 (2010).
- [29] V. W. Brar, M. S. Jang, M. Sherrott, S. Kim, J. J. Lopez, L. B. Kim, M. Choi, and H. Atwater, Hybrid surface-phonon-plasmon polariton modes in graphene/monolayer h-BN heterostructures, *Nano Lett.* **14**, 3876 (2014).
- [30] D. Grecu, Plasma frequency of the electron gas in layered structures, *Phys. Rev. B* **8**, 1958 (1973).
- [31] O. Y. Yermakov, A. I. Ovcharenko, M. Song, A. A. Bogdanov, I. V. Iorsh, and Y. S. Kivshar, Hybrid waves localized at hyperbolic metasurfaces, *Phys. Rev. B* **91**, 235423 (2015).
- [32] K. L. Koshelev and A. A. Bogdanov, Temperature-tunable semiconductor metamaterial, *Phys. Rev. B* **92**, 085305 (2015).
- [33] P. A. Belov, R. Marqués, S. I. Maslovski, I. S. Nefedov, M. Silveirinha, C. R. Simovski, and S. A. Tretyakov, Strong spatial dispersion in wire media in the very large wavelength limit, *Phys. Rev. B* **67**, 113103 (2003).
- [34] A. V. Chebykin, A. A. Orlov, A. V. Vozianova, S. I. Maslovski, Y. S. Kivshar, and P. A. Belov, Nonlocal effective medium model for multilayered metal-dielectric metamaterials, *Phys. Rev. B* **84**, 115438 (2011).
- [35] M. A. Gorlach and P. A. Belov, Effect of spatial dispersion on the topological transition in metamaterials, *Phys. Rev. B* **90**, 115136 (2014).
- [36] L. Ferrari, C. Wu, D. Lepage, X. Zhang, and Z. Liu, Hyperbolic metamaterials and their applications, *Prog. Quantum Electron.* **40**, 1 (2014).
- [37] P. Shekhar, J. Atkinson, and Z. Jacob, Hyperbolic metamaterials: Fundamentals and applications, *Nano Convergence* **1**, 14 (2014).
- [38] K. Y. Golenitskii, K. L. Koshelev, and A. A. Bogdanov, Tamm-Langmuir surface waves, *Phys. Rev. A* **94**, 043815 (2016).
- [39] A. Bogdanov and R. Suris, Effect of the anisotropy of a conducting layer on the dispersion law of electromagnetic waves in layered metal-dielectric structures, *JETP Lett.* **96**, 49 (2012).
- [40] D. Berreman, Optics in stratified and anisotropic media: 4×4 matrix formulation, *J. Opt. Soc. Am.* **62**, 502 (1972).
- [41] K. Manzoor, W. Waseer, Q. Naqvi, and M. Mughal, Goos-Hänchen shift observed from stratified medium, *Eur. Phys. J. D* **76**, 82 (2022).
- [42] H. M. Lai and S. W. Chan, Large and negative Goos-Hänchen shift near the Brewster dip on reflection from weakly absorbing media, *Opt. Lett.* **27**, 680 (2002).